Am J Cancer Res 2026;16(7):2763-2782
www.ajcr.us /ISSN:2156-6976/ajcr0171691

Original Article

MCPB-21 targets glycogenin-2 to regulate fatty acid oxidation and promote ferroptosis of breast cancer

Mengjie Mao[1*], Chunyu Wang[1*], Yingchun Lu[2], Qingxiu Tao[2], Long Zeng[1], Jing Li[3], Bin Liu[4]

[1]School of Medical and Life Sciences, Chengdu University of Traditional Chinese Medicine, Chengdu 611100, Sichuan, China; [2]School of Medicine, University of Electronic Science and Technology of China, Chengdu 610000, Sichuan, China; [3]Department of General Internal Medicine, Sichuan Cancer Hospital and Institute, Sichuan Cancer Center, School of Medicine, University of Electronic Science and Technology of China, Chengdu 610041, Sichuan, China; [4]Department of Medical Oncology, Sichuan Cancer Hospital and Institute, Sichuan Cancer Center, Affiliated Cancer Hospital of University of Electronic Science and Technology of China, Chengdu 610041, Sichuan, China. [*]Equal contributors.

Received January 26, 2026; Accepted June 30, 2026; Epub July 15, 2026; Published July 30, 2026

Abstract: This study systematically evaluated the anti-breast cancer potential and mechanisms of the cannabidiol (CBD) derivative MCPB-21. The structure of MCPB-21 was confirmed by nuclear magnetic resonance (NMR). The study analyzed differentially expressed genes associated with breast cancer using public databases and verified the binding affinity of MCPB-21 to glycogenin-2 (GYG2) through molecular docking. Additionally, the effects of MCPB-21 on apoptosis, invasion capacity, and lipid metabolism were evaluated in MDA-MB-231 and MCF-7 breast cancer cells using flow cytometry, Transwell invasion assays, cell proliferation assays, and Oil Red O staining. Western blot was employed to examine expression changes in proteins related to fatty acid β-oxidation and ferroptosis, including Acyl-CoA Oxidase 1 (ACOX1), ATP Binding Cassette Subfamily D Member 3 (ABCD3), ATP Binding Cassette Subfamily D Member 4 (ABCD4), Peroxisomal l-bifunctional enzyme (EHHADH), Carnitine palmitoyltransferase 1α (CPT1α), Glutathione Peroxidase 4 (GPX4), Solute Carrier Family 7 Member 11 (SLC7A11), and Acyl-CoA Synthetase Long Chain Family Member 4 (ACSL4). The role of fatty acid oxidation in ferroptosis was further analyzed using the ACOX1 inhibitor 10,12-Tricosadiynoic acid (500 nM). Additionally, the effects of MCPB-21 on fatty acid oxidation and ferroptosis were evaluated by interfering with GYG2 expression. Ferrostatin-1 (Fer-1) rescue experiments were conducted to verify the dependence of MCPB-21-induced cell death. Finally, the anti-tumor efficacy of various doses of MCPB-21 was compared to the control drug CBD. *In vitro* experimental results showed that MCPB-21 can affect the behavior of breast cancer cells by inducing cancer cell apoptosis, increasing reactive oxygen species (ROS) levels, and promoting lipid accumulation. At the same time, Western blot detection showed that MCPB-21 could downregulate key enzymes of fatty acid β-oxidation (ACOX1, ABCD3, ABCD4, EHHADH, CPT1α) and antioxidant factors (GPX4, SLC7A11), and upregulate the enzyme ACSL4 that promotes lipid peroxidation. Mechanistic studies further showed that MCPB-21 affects the expression of ACOX1 by regulating GYG2, inhibits fatty acid β-oxidation, and induces ferroptosis. At the same time, the combined use of ACOX1 inhibitors enhanced lipid accumulation and ROS levels, verifying its role in regulating fatty acid oxidation. In animal experiments, MCPB-21 (10 and 40 mg/kg) significantly inhibited the growth of nude mouse transplanted tumors, caused tumor tissue necrosis, inhibited the proliferation marker Ki67, and regulated the expression of ferroptosis-related proteins (GPX4 and SLC7A11 decreased, and ACSL4 increased). Immunohistochemical analysis showed that MCPB-21 had a stronger anti-tumor effect than CBD, mainly by regulating the fatty acid β-oxidation pathway to promote ferroptosis. In summary, MCPB-21 exhibits excellent anti-breast cancer potential. Its mechanism of action is mainly to achieve anti-tumor effects by inhibiting fatty acid β-oxidation and activating ferroptosis, which provides a theoretical basis and potential therapeutic strategy for the development of new anti-breast cancer drugs.

Keywords: Cannabidiol, MCPB-21, breast cancer, ferroptosis, fatty acid oxidation

Introduction

Breast cancer is a malignant tumor with the highest morbidity and mortality rate among women worldwide, and it seriously threatens women's lives and health [1, 2]. Notably, despite its lower incidence rate, breast cancer also affects men; in recent years, its unique epide-

https://doi.org/10.62347/DIDU5607

miological characteristics and prognostic outcomes have garnered widespread attention [3-5]. Although the current precision diagnosis and treatment model has opened up a new situation for breast cancer treatment, due to the high heterogeneity of tumors, there are still realistic problems in the clinic, such as large differences in survival prognosis, poor treatment efficacy in the late stage, and primary/secondary drug resistance [6, 7]. Therefore, identifying gene targets for accurate prediction of breast cancer survival prognosis and exploring potential leading therapeutic drugs are still research hotspots in breast cancer prevention and treatment.

Glycogenin-2 (GYG2) is a protein encoded by the human GYG2 gene, functioning as an autoglycosylase that facilitates the attachment of glucose monomers to itself, thereby forming short glucose polymers [8]. These polymers, or primers, serve as the initiation point for glycogen synthase to further elongate the glucose chain. GYG2 is integral to glycogen biosynthesis and has recently been implicated in metabolic disorders and cancer progression [9, 10]. Beyond its conventional role in glycogen synthesis, emerging evidence indicates that GYG2 may also participate in lipid metabolism through interactions with key enzymes in the fatty acid utilization pathway [11]. Specifically, the knockdown of GYG2 in adipocytes results in decreased expression of Acyl-CoA Oxidase 1 (ACOX1), a rate-limiting enzyme in peroxisomal fatty acid β-oxidation, thereby highlighting GYG2's regulatory role in fatty acid β-oxidation within adipocytes [12].

In breast cancer, ferroptosis is a potential therapeutic target [13]. Besides the Warburg effect of glycolysis in tumors, fatty acid metabolism is also a hot topic in the field of tumor research [14, 15]. Fatty acid oxidation (FAO) is a key energy source for tumor cells under nutritional stress; its metabolic imbalance can disrupt redox homeostasis and potentially increase the sensitivity of cells to ferroptosis [16, 17]. Ferroptosis is a form of iron-dependent cell death characterized by lipid peroxidation; as a highly promising cancer treatment strategy, it has attracted much attention in recent years. Unlike apoptosis or necrosis, ferroptosis is characterized by depletion of glutathione (GSH) and inactivation of glutathione peroxidase 4 (GPX4), leading to accumulation of lipid peroxides and ultimately cell membrane rupture [18, 19]. It is noteworthy that the metabolic reprogramming of cancer cells (especially the changes in FAO) is closely related to ferroptosis sensitivity [18]. Moreover, research on ferroptosis in breast cancer has become an important direction in the field of breast cancer research [20].

Natural products hold significant importance in drug development, particularly as leading active compounds with anti-tumor properties [21]. These compounds offer advantages such as structural diversity, rich biological activity, and natural origin, making them valuable resources for the discovery of novel anti-tumor drugs [22]. Cannabidiol (CBD), the second most abundant component of cannabis, has been shown to reduce the expression of the Id-1 gene in invasive human breast cancer cells, thereby inhibiting tumor cell proliferation and invasion [22-24]. Research by Sreevalsan *et al.* [25] demonstrated that CBD can inhibit prostate cancer cells in a concentration-dependent manner. Despite these promising findings, CBD has not been adopted in the clinical treatment of cancer patients due to its high lipophilicity, poor solubility in the gastrointestinal system, and susceptibility to first-pass metabolism in the liver [26]. Studies indicate that the liver metabolizes CBD at a rate of 65% to 70%, resulting in extremely low bioavailability following oral administration [27]. Consequently, CBD was chemically modified to develop cannabidiol derivatives, leading to the identification of a novel compound, MCPB-21, which exhibits cytotoxic effects on breast cancer cells.

This study aims to elucidate the interaction between FAO and ferroptosis in breast cancer mediated by ACOX1 by targeting GYG2 by MCPB-21 and validate MCPB-21 as a first-in-class GYG2 inhibitor with therapeutic potential.

Materials and methods

This study was approved by the Experimental Animal Ethics Committee of West China Hospital, Sichuan University, with the ethics filing number: 20250528007.

CBD synthesis of MCPB-21

The compound cannabidiol (CBD, 2.0 g, 1.0 equivalent) was dissolved in 150 mL of metha-

nol as the solvent. Subsequently, 1-methylpiperidin-4-amine (1.8 g, 2.5 equivalents) and formaldehyde (40% aqueous solution, 1.5 mL, 2.5 equivalents) were added with continuous magnetic stirring. The reaction was conducted under a nitrogen atmosphere at 80°C for 16 hours. The progress of the reaction was monitored using thin-layer chromatography (TLC) in conjunction with ultraviolet (254 nm UV) analysis. Upon completion of the reaction, the mixture was allowed to cool to room temperature and concentrated under reduced pressure to remove the solvent. The crude product was dissolved in 100 mL of ethyl acetate (EA) and washed three times with 100 mL of saturated saline solution. The organic phase was collected and subjected to separation and purification *via* silica gel column chromatography, using a petroleum ether to ethyl acetate ratio of 10:1. This process yielded a light yellow foamy solid weighing 1.12 g, corresponding to a yield of 30%. The structure of the compound was characterized using nuclear magnetic resonance (NMR) spectroscopy.

Bioinformatics analysis

In this study, the differences in GYG2 gene expression between cancerous and paracancerous tissues of breast cancer patients were analyzed through the UALCAN platform (https://ualcan.path.uab.edu/index.html) to assess the changes in its expression in breast cancer. Kaplan-Meier survival analysis (https://kmplot.com/analysis/) was then used to compare the survival of patients with different GYG2 expression levels and to explore its correlation with patient prognosis.

Molecular docking

Autodock4 was employed for semi-flexible molecular docking between ligands and receptors. MCPB-21 served as the small molecule ligand for docking with the GYG2 protein. The MCPB-21 structure was created and converted to 3D using Chem3D 20.0 (Perkin Elmer), then saved as a mol2 file post-energy optimization. The GYG2 protein receptor's PDB file (PDB: 4UEG) (https://www.rcsb.org/annotations/4UEG) was downloaded from the PDB website, and water molecules along with the original ligands were removed using Discovery Studio (https://www.discover.3ds.com). The protein receptor underwent hydrogenation, and the file format was changed using Autodock4 (https://autodock.scripps.edu/download-autodock4/), which also determined the active pocket and executed the docking.

Cell culture

Human breast cancer cells MCF-7 (iCell-h129, iCell, Shanghai, China) were cultured in RPMI-1640 (iCell-h129-001b, iCell, Shanghai, China) medium containing 10% fetal bovine serum (C04001-500, Vivacell, Shanghai, China), and MDA-MB-231 (iCell-h133, iCell, Shanghai, China) were cultured in L15 (PM151010, Procell, Shanghai, China) medium containing 10% fetal bovine serum in an incubator with 95% saturated humidity, 37°C, and 5% CO_2.

Transfection experiment

A 1.5 mL centrifuge tube was supplemented with 360 μL of 1X riboFECT™ MCP Buffer to dilute 15 μL of siRNA, followed by gentle mixing. Subsequently, 36 μL of riboFECT™ MCP Reagent was added, mixed gently, and incubated at room temperature for 15 minutes to prepare the riboFECT™ MCP transfection complex, achieving a final siRNA concentration of 50 nM. Once the cells adhered to the surface, the supernatant in the well was aspirated, and the riboFECT™ MCP transfection complex was combined with an appropriate volume of complete medium lacking dual antibodies. This mixture was added to the well plate and incubated at 37°C with 5% CO_2. The transfection sequence: Si-GYG2 Sense-GUUGGACUCUCACUCACUATT, Si-GYG2 Antisense-UAGUGAGUGAGAGUCCAACTT. Si-NC Sense-UUCUCCGAACGUGUCACGUTT; Si-NC Antisense-ACGUGACACGUUCGGAGAATT-3'. The siRNAs used in this study were purchased from Shanghai GenePharma Co., Ltd. (Shanghai, China).

Flow cytometry apoptosis assay

Cells from the logarithmic growth phase of MDA-MB-231 and MCF-7 were collected, and the cell density was adjusted to 2×10^5 cells per well. The cells were inoculated into 6-well plates at a volume of 2 mL per well and cultured at 37°C and 5% CO_2. After the transfection experiment was completed, the cells were digested, washed, and collected. The cells were resuspended in 500 μL of binding buffer (Binding

Buffer), and 5 μL of Annexin V-APC (KGA1107, Keji Biology, Jiangsu, China) was added and thoroughly mixed; then 5 μL of PI was added and thoroughly mixed. The cells were incubated at room temperature in the dark for 15 minutes. After incubation, cell apoptosis in each group was analyzed by flow cytometry.

Transwell assay

The MDA-MB-231 and MCF-7 cells were enzymatically digested and centrifuged, and then resuspended in serum-free medium. Subsequently, the cells were seeded at a density of 5×10^5 cells per well in the upper chamber of the Transwell chamber (3422, Corning, New York, USA), with each well containing 200 μL of medium. 600 μL of medium containing 20% serum was added to the lower chamber. The Transwell chamber was placed under specific conditions (37°C, 5% CO_2) for 48 h of culture. After the culture was completed, the upper chamber was carefully removed and washed multiple times with PBS. The cells were then fixed using 4% paraformaldehyde for 30 minutes and stained with crystal violet (JC3913, Bomei, Hefei, China) for 5 minutes. Non-migrated cells in the upper chamber were gently removed using a PBS-moistened cotton swab. Subsequently, five random fields of view at 200× magnification were selected to observe and quantify the number of cells that had traversed the chambers.

Oil Red O staining

MCF-7 and MDA-MB-231 cells were seeded in 6-well plates (3×10^5/well) and cultured for 24 hours. The cells were then given drugs according to the experimental groups. Group 1: Control, 5 μM MCPB-21, 10 μM MCPB-21, 20 μM MCPB-21. Group 2: Control, MCPB-21, 10,20-Tricosadiynoic acid, MCPB-21 + 10,20-Tricosadiynoic acid. Group 3: Control, MCPB-21, MCPB-21 + si-NC, MCPB-21 + si-GYG2. After the drug administration, the cells were washed with PBS, fixed with 4% paraformaldehyde for 20 minutes, rinsed with distilled water, and briefly soaked in 60% isopropanol (20-30 s). Then, the cells were stained with freshly prepared Oil Red O staining solution (G1262, Solarbio, Beijin, China) for 15 minutes, rinsed with 60% isopropanol to remove excess dye, and finally washed with distilled water 2-5 times [28]. The lipid deposition was observed under a microscope and photographed.

Flow cytometry for ROS

MCF-7 and MDA-MB-231 cells were cultured in 6-well plates, with 1×10^6 cells from each group subjected to two washes with PBS. Subsequently, the cells were incubated with a probe, prepared as a 500 μl suspension containing 5 mol/L DCFH-DA (78EA10007, Shanghai QIFA, Shanghai, China), and allowed to react for 30 minutes in the dark at 37°C. After incubation of MDA-MB-231 and MCF-7 cells, they were washed twice with PBS. The changes in reactive oxygen species (ROS) among the groups were evaluated using the FITC channel, and the changes in ROS levels were quantitatively analyzed based on the optical density values measured by the FITC channel.

Western blot assay

MCF-7 and MDA-MB-231 cells, as well as tumor tissue from transplanted tumors, were collected for protein analysis. Total proteins from each group were extracted using RIPA protein lysis buffer, and the protein concentration was determined by the BCA method; subsequently, 50 μg of protein from each well was separated by 10% SDS-PAGE and transferred to a PVDF membrane for electrophoretic separation. These membranes were then incubated with a TBST-blocking solution containing 5% skim milk at room temperature for 2 hours. Following this, the membranes were incubated overnight at 4°C with primary antibodies: ABCD3 (ATP Binding Cassette Subfamily D Member 3, Huabio, HA721969, 1:2000, Hangzhou, China), ABCD4 (ATP Binding Cassette Subfamily D Member 4, Huabio, ER62551, 1:2000, Hangzhou, China), ACOX1 (Zenbio, R23371, 1:1000, North Carolina, USA), ACSL4 (Acyl-CoA Synthetase Long Chain Family Member 4, Proteintech, 22401-1-AP, 1:2000, Wuhan, China), CPT1α (Carnitine palmitoyltransferase 1α, Bioss, BS-23779R, 1:2000, Beijin, China), EHHADH (Peroxisomal l-bifunctional enzyme, Cusabio, CSB-PA600104LA01HU, 1:2000, Wuhan, China), GPX4 (Abclonal, A1933, 1:15000, Wuhan, China), GYG2 (Proteintech, 13150-1-AP, 1:1000, Wuhan, China), SLC7A11 (Solute Carrier Family 7 Member 11, Abclonal, A2413, 1:1000, Wuhan, China), and β-actin (Abclonal, AC026, 1:50000, Wuhan, China). Post-incubation, the membranes were washed with TBST and then incubated with a secondary IgG anti-

body (Affinity, S0001, 1:8000, Wuhan, China) at room temperature for 2 hours. After further washing with TBST, the analysis proceeded [29].

Animal experiments

8-week-old BALB/c female nude mice (18 ± 2 g) were used for subcutaneous tumor xenograft experiments. The mice were raised with free access to food and water, and the lighting conditions were a 12-h light/dark cycle. The mice were divided into control group, 10 mg/kg MCPB-21 group, 40 mg/kg MCPB-21 group, and 10 mg/kg CBD group. A total of 1×10^6 MDA-MB-231 breast cancer cells were inoculated into the right lower limb of mice. Upon reaching an average tumor volume of 50-100 mm^3, the mice were randomly allocated into four groups (n = 5 per group). The experimental groups received intraperitoneal injections of MCPB-21 at doses of 10 and 40 mg/kg, or 10 mg/kg of CBD [30], administered once daily for 21 days. The control group received equivalent volumes of saline. The health status and behavior of the nude mice were monitored daily. Body weight and tumor dimensions were monitored every three days following the initiation of treatment. Animals are humanely euthanized once they reach predetermined humane endpoints [31-33]. Humane endpoints are defined as a tumor measurement of ≥ 1.5 cm in any dimension accompanied by a body weight loss of > 20% from baseline, or a body weight loss of 10% accompanied by severe signs of clinical distress (e.g., thinning fur, loss of appetite, or reduced vitality). Mice reaching these endpoints are euthanized [34]. Upon conclusion of the experiment, both tissue and tumor weights were recorded, and tumor volumes were measured and documented photographically. Following the experimental procedures, mice were anesthetized *via* an intraperitoneal injection of sodium pentobarbital (50 mg/kg) and subsequently euthanized by cervical dislocation. Euthanasia was confirmed by the cessation of cardiac and respiratory activity, alongside the loss of corneal reflexes. Subsequently, tumor tissues were harvested for further analysis. Animal experiments were conducted in accordance with Animal Research: Reporting of In Vivo Experiments.

H&E staining

Tumor tissues from nude mice in each group were collected and fixed in 4% neutral formaldehyde solution for 24 hours. The tissues were then dehydrated with alcohol, cleared with xylene, and embedded in paraffin wax. Paraffin-embedded tissue blocks were sectioned into 5 μm-thick slices using a microtome, mounted onto glass slides, and dried. Tissue sections were first stained with hematoxylin for 5 minutes, followed by differentiation with 1% ethanol acid solution (H9627, Sigma-Aldrich, USA) for 3 seconds; subsequently, they were counterstained with eosin solution (YE2080, Bomeibio, Hefei, China) for 1 minute. Finally, after dehydration, clearing, and drying, the sections were coverslipped with neutral gum [35]. The prepared slides were then examined and imaged under a microscope.

Immunohistochemical staining

Transplanted tumors from each group of nude mice were collected and fixed in 4% neutral formaldehyde solution for 24 hours. The tissues were then dehydrated with alcohol, cleared with xylene, and embedded in paraffin wax. Paraffin-embedded tissue blocks were sectioned into 5 μm thick slices using a microtome, mounted onto glass slides, and dried. Tumor sections from each group were treated with microwave irradiation in citrate buffer, followed by incubation with 3% hydrogen peroxide to block endogenous peroxidase activity, and then blocked with bovine serum blocking solution. Primary antibodies including Ki67 (1:400, HA721115, HUABIO, Wuhan, China), ACSL4 (1:50, Proteintech, 81196-1-RR, Wuhan, China), GPX4 (1:200, Proteintech, 67763-1-Ig, Wuhan, China), and SLC7A11 (1:100, Proteintech, 26864-1-AP, Wuhan, China) were added and incubated overnight at 4°C. Subsequently, the sections were incubated with HRP-conjugated secondary antibody (1:100, GB23301, Servicebio, Wuhan, China) at room temperature for 30 minutes, followed by addition of DAB substrate and incubation at room temperature for 10 minutes. Sections were counterstained with hematoxylin for 3 minutes, rinsed with tap water, and differentiated with hematoxylin differentiation solution for 3 seconds [36]. The sections were then sealed with a mounting medium. Images of the sections were captured using a microscopic camera system, and all collected images were analyzed using the ImageJ software.

Statistical analysis

Statistical analyses of the experimental results were conducted using SPSS software version 22.0 (version 22.0, SPSS Inc., Chicago, IL, USA). The Shapiro-Wilk test was used to assess normality, and data are presented as mean ± standard deviation ($\bar{x}$ ± s). Multiple-group comparisons were performed using one-way ANOVA (Levene's test of variance); the Tukey test was applied when variances were homogeneous, while Welch's ANOVA followed by Tamhane's T2 was used when variances were heterogeneous. A *p*-value of less than 0.05 was considered indicative of statistical significance.

Results

Synthesis and characterization of MCPB-21

Synthetic route of MCPB-21 from CBD, 1-methylpiperidine-4-methylamine, and formaldehyde (**Figure 1A**). Nuclear Magnetic Resonance (NMR) spectrum of MCPB-21: ^{1}H NMR (400 MHz, DMSO-d6) δ 5.01 (s, 1H), 4.76 (s, 4H), 4.40 (d, J = 5.7 Hz, 2H), 3.88 (d, J = 5.1 Hz, 4H), 3.77 (d, J = 12.6 Hz, 1H), 2.84 (t, J = 10.1 Hz, 1H), 2.74 (d, J = 9.8 Hz, 4H), 2.28 (d, J = 29.1 Hz, 3H), 2.11 (s, 6H), 1.89 (d, J = 16.8 Hz, 2H), 1.78 (d, J = 9.6 Hz, 8H), 1.64 (s, 2H), 1.57 (s, 3H), 1.54 (s, 3H), 1.42 (d, J = 7.2 Hz, 4H), 1.32 (s, 7H), 0.87 (d, J = 6.7 Hz, 3H) (**Figure 1B**). The above experimental results show that MCPB-21 was successfully synthesized.

Expression of GYG2 in breast cancer and its targeting relationship with MCPB-21

The analysis of differential gene expression between cancerous and adjacent non-cancerous tissues in breast cancer patients, as conducted using UALCAN (uab.edu), revealed a significant downregulation of the GYG2 gene in cancerous tissues (**Figure 2A**). Furthermore, survival prognosis analysis using the Kaplan-Meier plotter (kmplot.com) demonstrated a markedly reduced survival period in patients exhibiting low GYG2 expression levels (log-rank P = 0.045) (**Figure 2B**). These findings suggest that GYG2 may play a pro-oncogenic role in the pathogenesis of breast cancer. In previous studies, we found that MCPB-21 can inhibit the proliferation of breast cancer cells. To evaluate the regulation of MCPB-21 on GYG2, molecular docking experiments were conducted. The results showed that MCPB-21 formed hydrogen bond interactions with residue ARG30; MCPB-21 formed van der Waals interactions with residues LEU74, LYS78, SER111, ILE66, THR254, VAL255, LEU108, and GLU81; MCPB-21 formed hydrogen bonds with residues LEU77, SER208, and GLY207; and MCPB-21 formed Pi-Cation interactions with residue HIS31 (**Figure 2C** and **2D**). Molecular docking results showed that the binding energy of MCPB-21 and GYG2 was -10 kcal/mol, indicating that MCPB-21 bound well to GYG2.

Effects of MCPB-21 on cell behavior of breast cancer cells

As shown in **Figure 3A** and **3B**, compared with the control group, 5, 10, and 20 μM MCPB-21 could induce apoptosis of breast cancer cells MDA-AB-231 and MCF-7. Compared with the control group, 5, 10, and 20 μM MCPB-21 could promote the invasion ability of MDA-AB-231 and MCF-7 (**Figure 3C** and **3D**). Oil red O staining showed that compared with the control, lipid droplet formation was observed in MDA-AB-231 and MCF-7 treated with 10 and 20 μM MCPB-21 (**Figure 3E** and **3F**). Flow cytometry detected ROS. Compared with the control group, the ROS levels of MDA-AB-231 and MCF-7 increased after 5, 10, and 20 μM MCPB-21 (**Figure 3G** and **3H**).

Effects of MCPB-21 on fatty acid β-oxidation and ferroptosis

Figure 4A-C shows the enzymes related to the fatty acid β-oxidation metabolic pathway in breast cancer. Compared with the control group, 5, 10, and 20 μM MCPB-21 can inhibit the expression of ACOX1, ABCD3, ABCD4, EHHADH, and CPT1α in MDA-AB-231 and MCF-7 cells. In terms of ferroptosis response elements, compared with the control group, 5, 10, and 20 μM MCPB-21 inhibited the expression of GPX4 and SLC7A11 in MDA-AB-231 and MCF-7, and upregulated the expression of ACSL4 in MDA-AB-231 and MCF-7 (**Figure 4D-F**).

MCPB-21 regulates ferroptosis via ACOX1 in breast cancer by modulating fatty acid β-oxidation

As shown in **Figure 5A** and **5B**, the Oil Red O-stained lipid droplets of MDA-AB-231 and

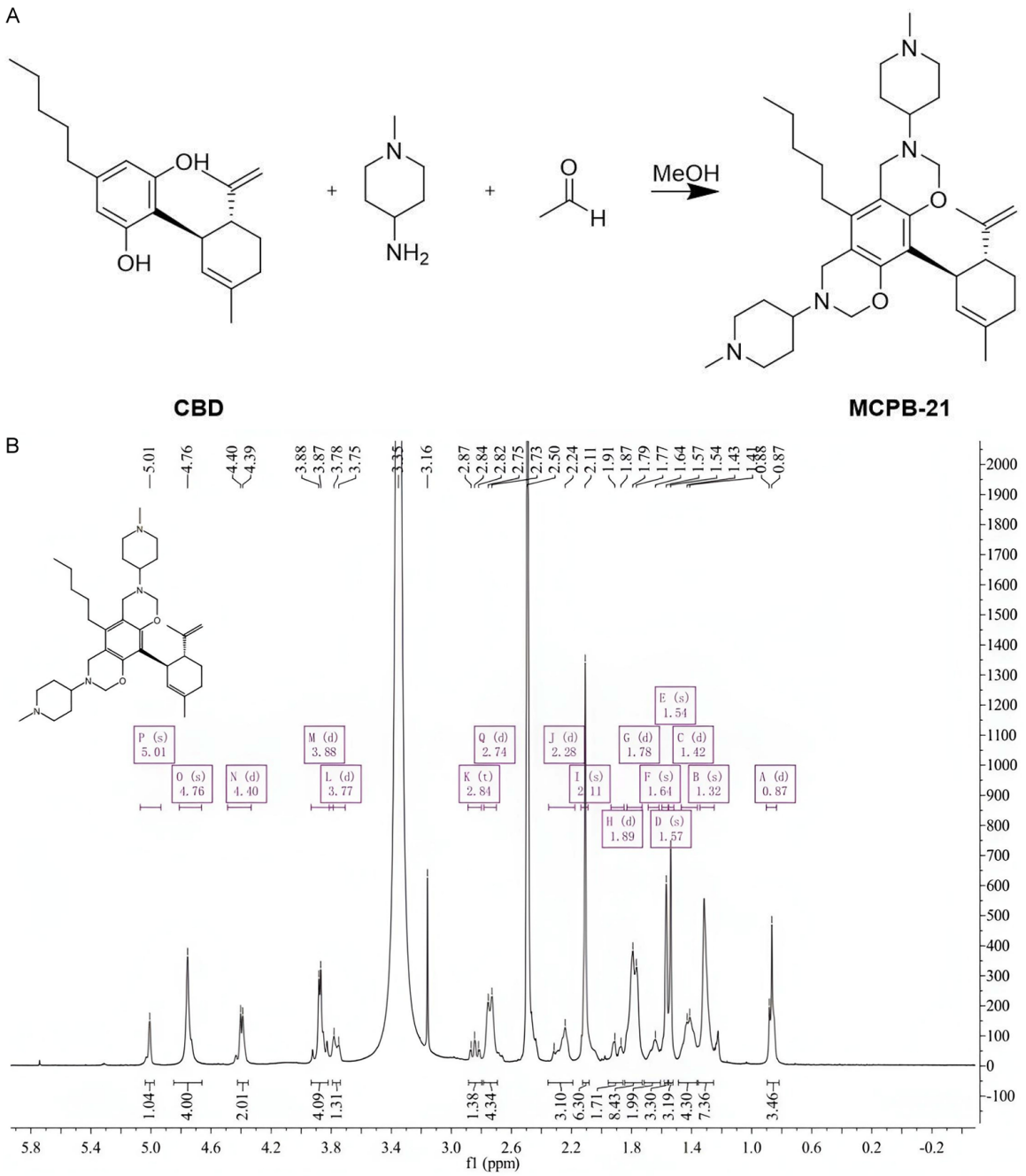

Figure 1. Synthesis and identification of MCPB-21 synthesized from CBD. A. Route of MCPB-21 synthesized from CBD. B. H-NMR spectrum of MCPB-21.

MCF-7 increased after the treatment of MCPB-21 and 500 nM 10,12-Tricosadiynoic acid compared with the control group. Compared with MCPB-21, the stained lipid droplets increased after combining MCPB-21 and 10,12-Tricosa diynoic acid. An investigation into the effects of MCPB-21 and 10,12-Tricosadiynoic acid revealed a significant increase in ROS production compared to the control group. This increase was further amplified following the co-incubation of MDA-AB-231 and MCF-7 cells with MCPB-21 and 10,12-Tricosadiynoic acid, as illustrated in **Figure 5C** and **5D**. When we shifted our focus to the protein levels, compared with the control group, MCPB-21, and 10,12-Tricosadiynoic acid inhibited the expres-

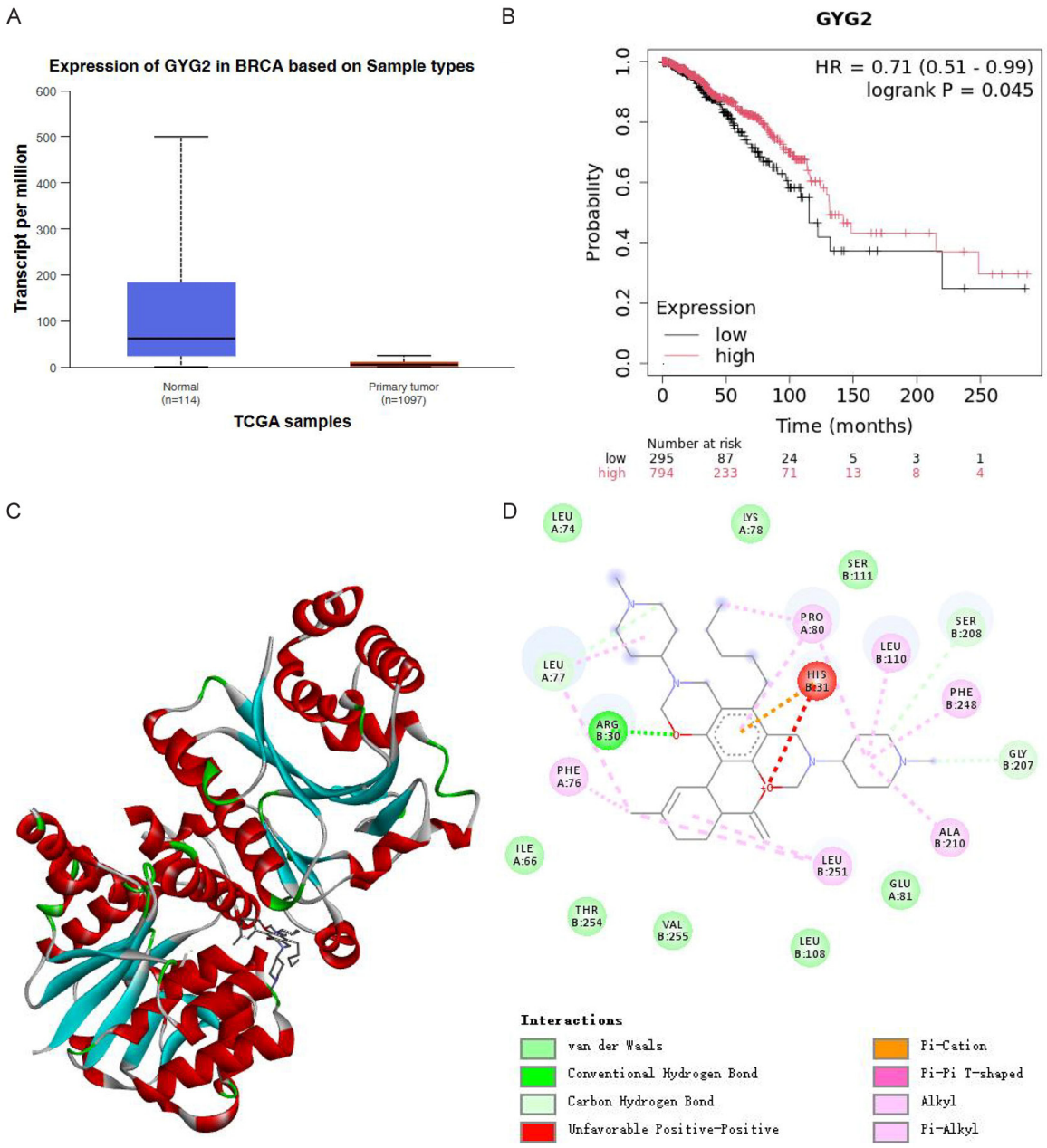

Figure 2. Survival analysis of GYG2 and breast cancer patients and validation of its targeting relationship with MCPB-21. A. Expression of GYG2 in breast cancer. B. Relationship between GYG2 expression and patient survival. C, D. Molecular docking results of MCPB-21 and GYG2.

sion of ACOX1, ABCD3, ABCD4, EHHADH, and CPT1α in MDA-AB-231 and MCF-7, and the combination of the two further decreased the expression of these proteins (**Figure 5E-G**). Evidently, from **Figure 5H-J**, MCPB-21 and 10,12-Tricosadiynoic acid-induced ferroptosis in MDA-AB-231 and MCF-7, and the combination of MCPB-21 and 10,12-Tricosadiynoic acid increased ferroptosis in breast cancer cells (**Figure 5H-J**).

MCPB-21 modulates ACOX1 via GYG2 to alter fatty acid β-oxidation and ferroptosis in breast cancer

In MDA-AB-231 and MCF-7, 5, 10, and 20 μM MCPB-21 induced the expression of GYG2 compared with the control group (**Figure 6A** and **6B**). Additionally, GYG2 was silenced to observe the effect of MCPB-21 on fatty acid β-oxidation and ferroptosis in breast cancer (supplementa-

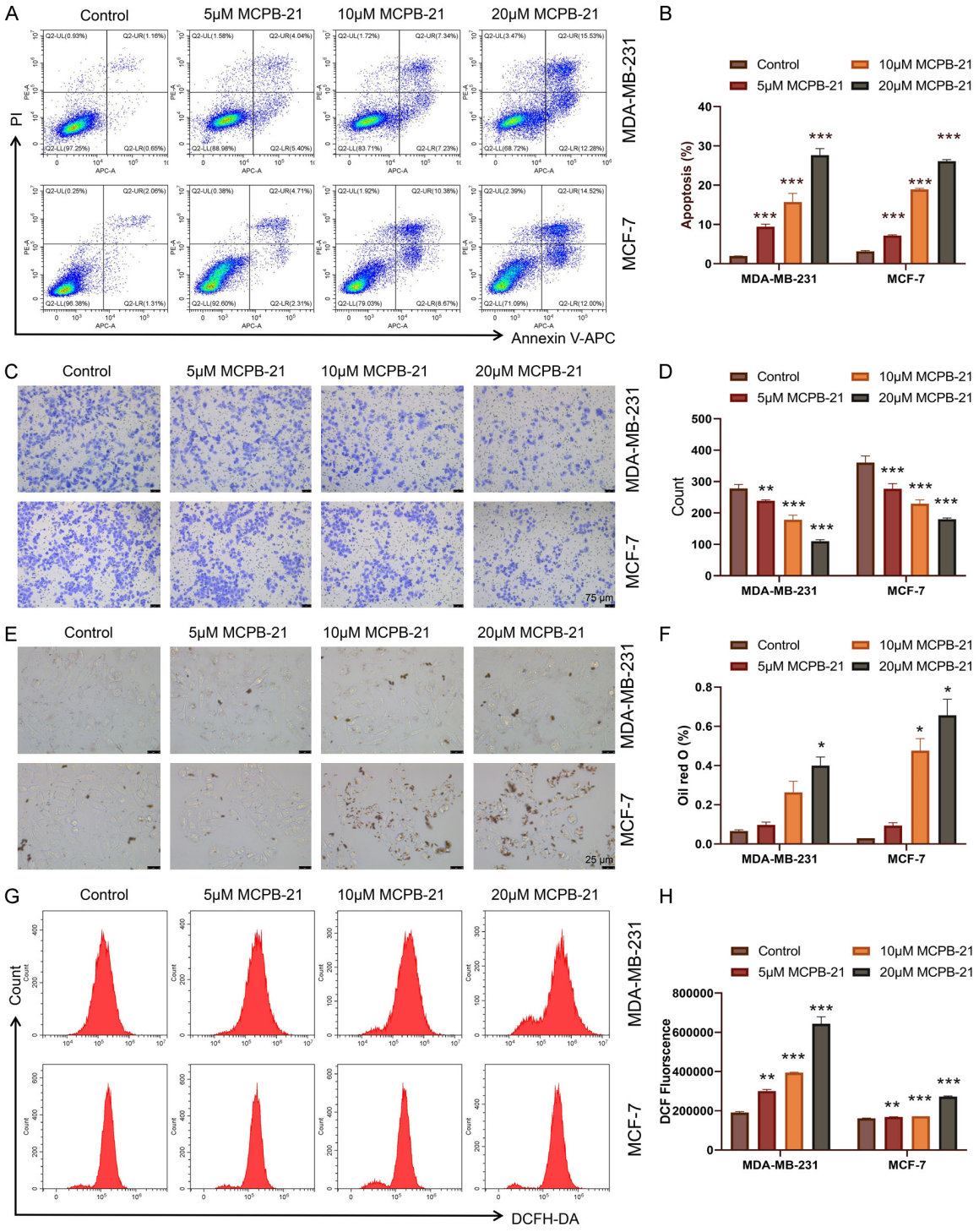

Figure 3. Effects of MCPB-21 on cell behavior of MDA-AB-231 and MCF-7. A. Flow cytometry was used to detect apoptosis of MDA-AB-231 and MCF-7. B. Statistical results of apoptosis of MDA-AB-231 and MCF-7. C. Transwell assay was used to detect the invasion ability of MDA-AB-231 and MCF-7. D. Statistical results of invasion of MDA-AB-231 and MCF-7. E. Oil red staining results of MDA-AB-231 and MCF-7. F. Statistical results of Oil red staining of MDA-AB-231 and MCF-7. G. Representative images of ROS of MDA-AB-231 and MCF-7. H. Statistical results of ROS of MDA-AB-231 and MCF-7. Compared with control group, $*P < 0.05$, $**P < 0.01$, and $***P < 0.001$.

ry). As shown in **Figure 6C** and **6D**, compared with the control group, the lipid droplets of breast cancer cells increased after MCPB-21 incubation. Compared with the MCPB-21 group,

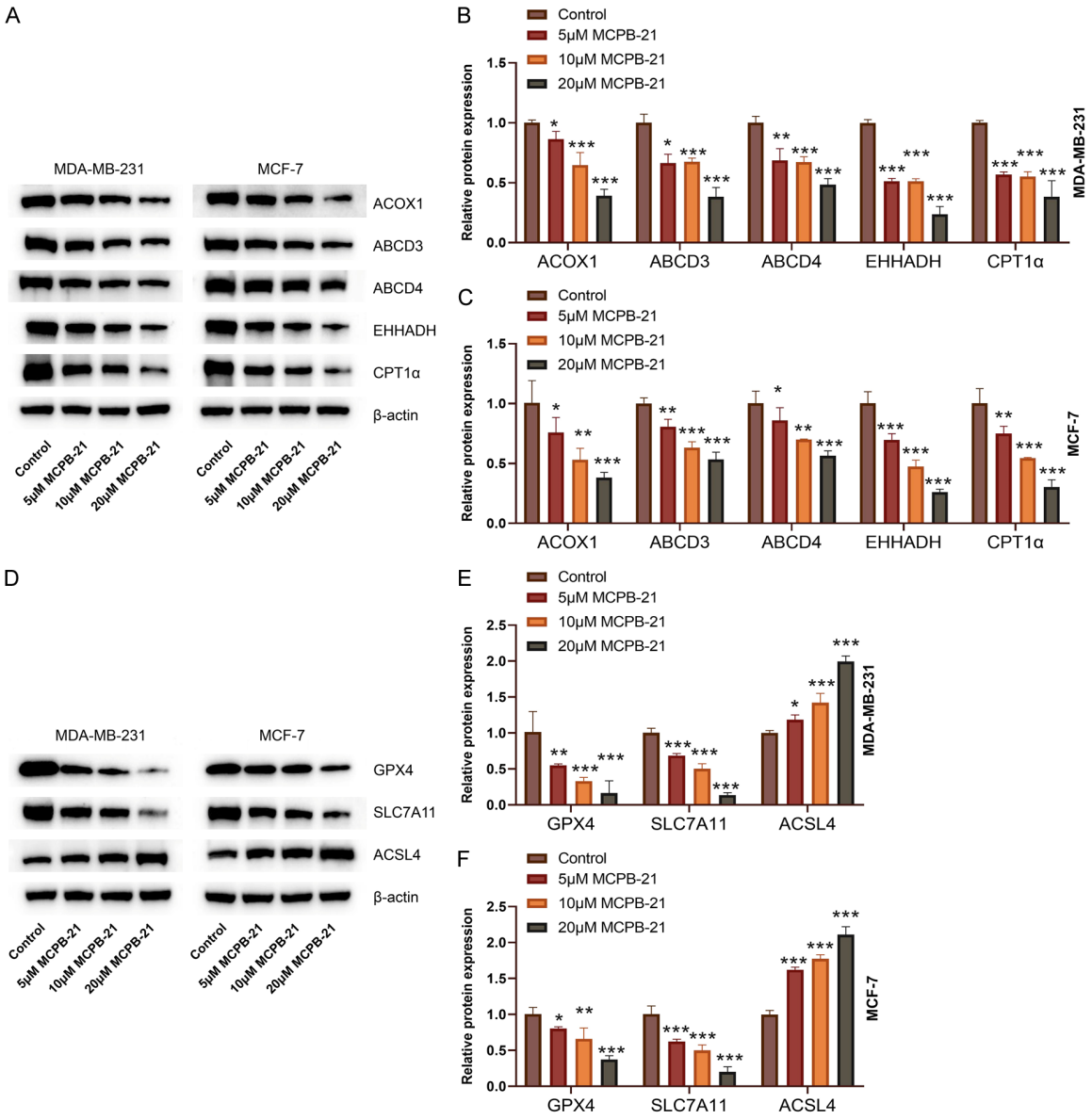

Figure 4. MCPB-21 inhibits fatty acid β-oxidation and induces ferroptosis in breast cancer cells of MDA-AB-231 and MCF-7. (A) Representative protein bands of ACOX1, ABCD3, ABCD4, EHHADH, and CPT1α in MDA-AB-231 and MCF-7. Relative expression statistics of ACOX1, ABCD3, ABCD4, EHHADH, and CPT1α in MDA-AB-231 (B) and MCF-7 (C). (D) Representative protein bands of GPX4, SLC7A11, and ACSL4 in MDA-AB-231 and MCF-7. Relative expression statistics of GPX4, SLC7A11, and ACSL4 in MDA-AB-231 (E) and MCF-7 (F). Compared with control group, $*P < 0.05$, $**P < 0.01$, and $***P < 0.001$.

MCPB-21 combined with si-NC did not affect the lipid droplet formation of breast cancer, and MCPB-21 combined with si-GYG2 reduced lipid droplets. Probing into ROS, compared with the control group, breast cancer ROS was enhanced after MCPB-21 treatment. On the contrary, ROS was attenuated after silencing GYG2 based on MCPB-21 (**Figure 6E** and **6F**). Moreover, compared with the control group, the expression of ACOX1, ABCD3, ABCD4, EHHADH, and CPT1α was increased after MCPB-21 incubation of breast cancer cells, and the expression of these proteins was reduced after transfection of si-GYG2 (**Figure 6G-I**). Remarkably, MCPB-21 inhibited the expression of GPX4 and SLC7A11 in breast cancer cells and induced the expression of ACSL4. After silencing GYG2, the expression of GPX4 and SLC7A11 increased, and the

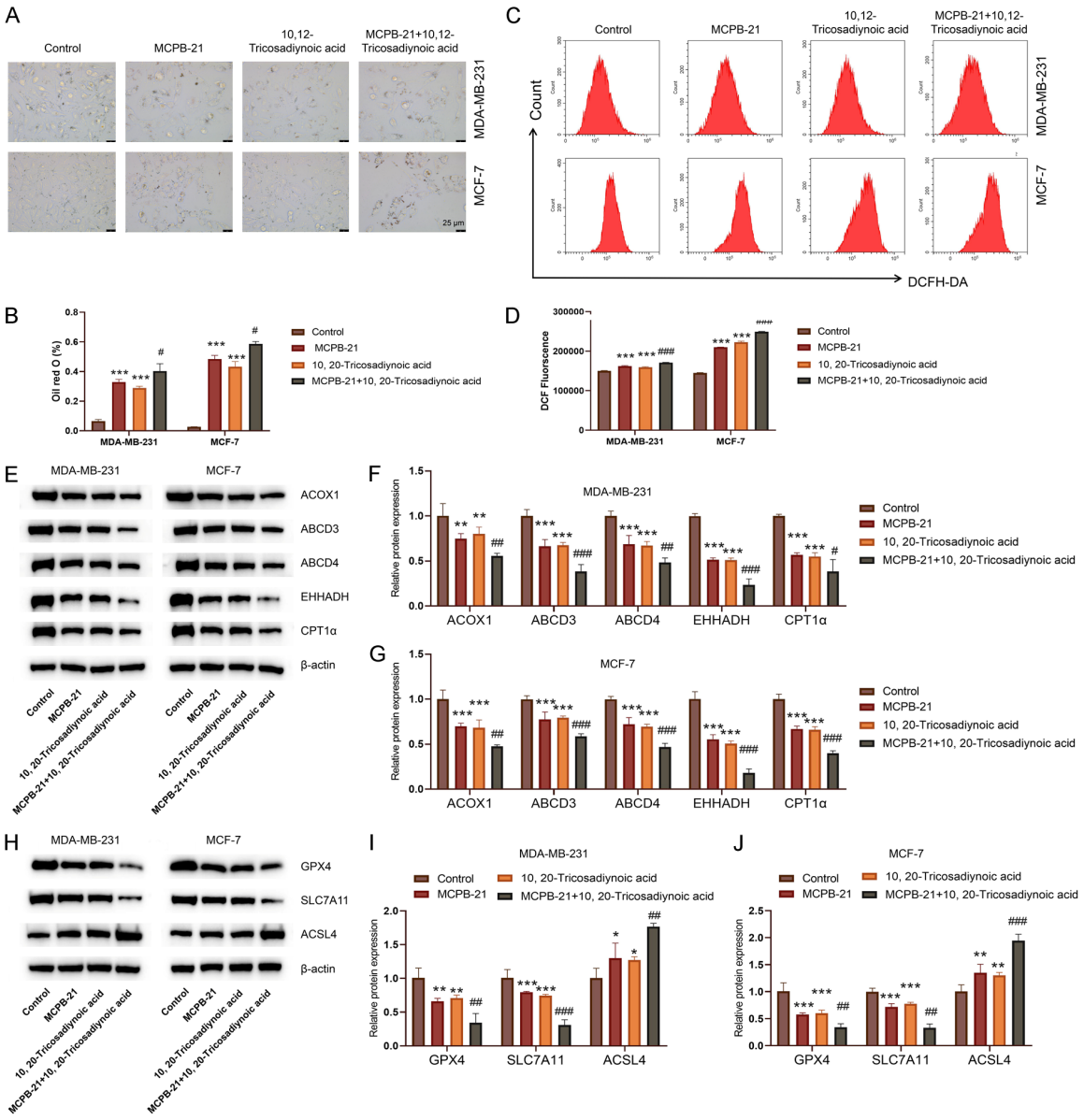

Figure 5. MCPB-21 induces ferroptosis by regulating fatty acid β-oxidation through ACOX1. (A) Oil red staining results of MDA-AB-231 and MCF-7. (B) Statistical results of Oil red staining of MDA-AB-231 and MCF-7. (C) Representative images of ROS in MDA-AB-231 and MCF-7. (D) Statistical results of ROS in MDA-AB-231 and MCF-7. (E) Representative protein bands of ACOX1, ABCD3, ABCD4, EHHADH, and CPT1α in MDA-AB-231 and MCF-7. Relative expression statistics of ACOX1, ABCD3, ABCD4, EHHADH, and CPT1α in MDA-AB-231 (F) and MCF-7 (G). (H) Representative protein bands of GPX4, SLC7A11, and ACSL4 in MDA-AB-231 and MCF-7. Relative expression of GPX4, SLC7A11, and ACSL4 in MDA-AB-231 (I) and MCF-7 (J). Compared with the control group, $*P < 0.05$, $**P < 0.01$, and $***P < 0.001$. Compared with MCPB-21, $\#P < 0.05$, $\#\#P < 0.01$, and $\#\#\#P < 0.001$.

expression of ACSL4 decreased (**Figure 6J-L**). These experimental results suggest that MCPB-21 regulates GYG2 to affect ACOX1 and inhibit fatty acid oxidation in breast cancer cells, and ROS enrichment induces cell ferroptosis.

MCPB-21 inhibits breast cancer cell growth by inducing ferroptosis

Flow cytometry analysis of cell death revealed (**Figure 7A** and **7B**) that, compared to the con-

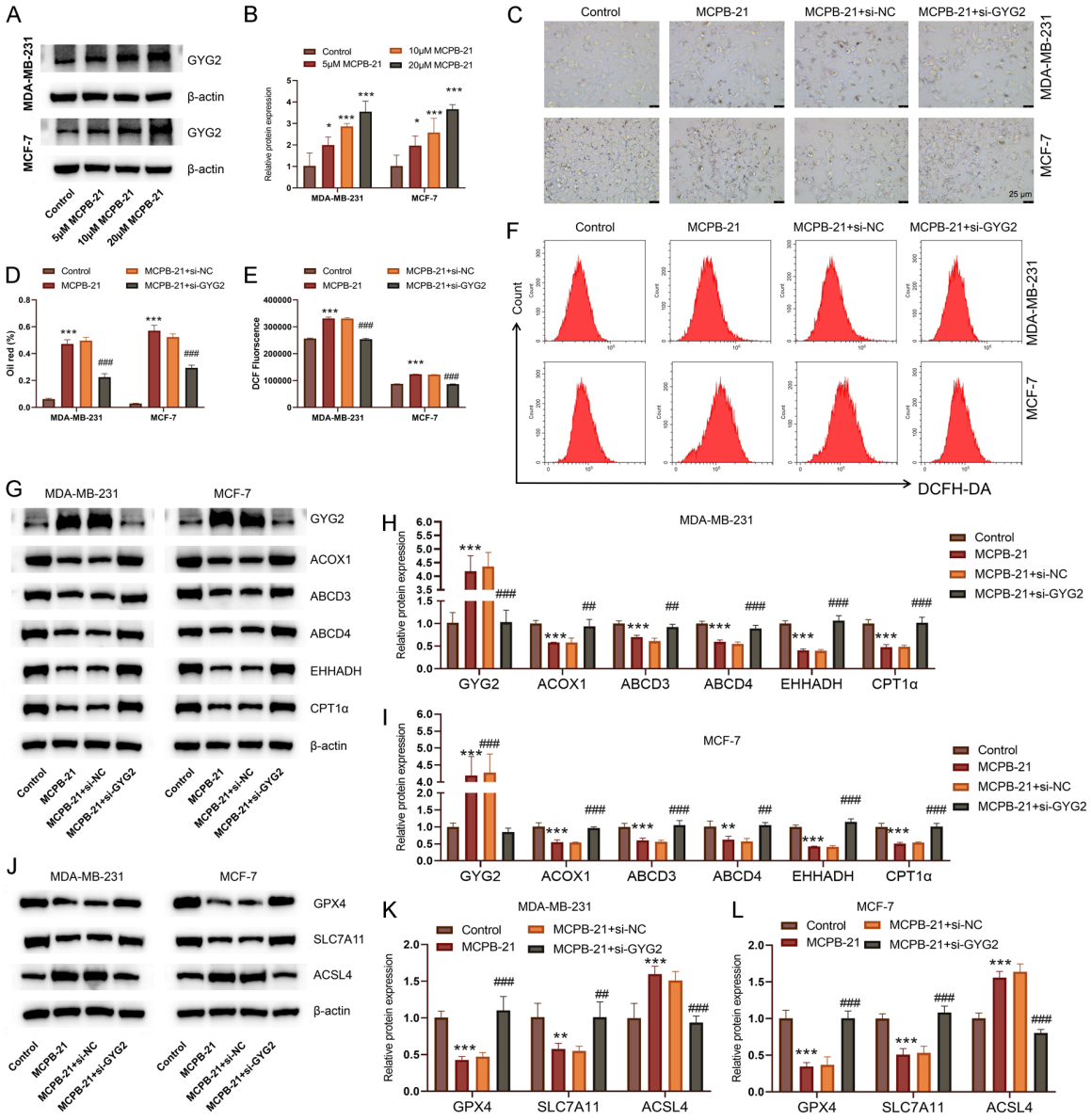

Figure 6. MCPB-21 regulates fatty acid oxidation and ferroptosis in breast cancer cells *via* GYG2. (A) Representative bands of GYG2 in MDA-AB-231 and MCF-7. (B) Relative expression statistics of GYG2. (C) Oil red staining results of MDA-AB-231 and MCF-7. (D) Oil red staining results of MDA-AB-231 and MCF-7. (E) ROS statistics of MDA-AB-231 and MCF-7. (F) Representative images of ROS in MDA-AB-231 and MCF-7. (G) Representative protein bands of ACOX1, ABCD3, ABCD4, EHHADH, and CPT1α in MDA-AB-231 and MCF-7. Relative expression statistics of ACOX1, ABCD3, ABCD4, EHHADH, and CPT1α in MDA-AB-231 (H) and MCF-7 (I). (J) Representative protein bands of GPX4, SLC7A11, and ACSL4 in MDA-AB-231 and MCF-7. Statistical results of relative expression of GPX4, SLC7A11, and ACSL4 in MDA-AB-231 (K) and MCF-7 (L). Compared with the control group, **P* < 0.05, ***P* < 0.01, and ****P* < 0.001. Compared with MCPB-21, #*P* < 0.05, ##*P* < 0.01, and ###*P* < 0.001.

trol group, treatment with 10 μM MCPB-21 significantly increased the proportion of dead cells in both MDA-MB-231 and MCF-7 cell lines. However, when combined with the 1 μM ferroptosis inhibitor Fer-1, the proportion of MCPB-21-induced cell death decreased markedly, providing preliminary evidence that the cell death induced by MCPB-21 is ferroptosis-dependent. Detection using the DCFH-DA probe demonstrated (**Figure 7C** and **7D**) that the fluorescence intensity in the MCPB-21-treated group was higher than that in the control group, indicating a substantial increase in intracellular ROS levels. Upon the addition of

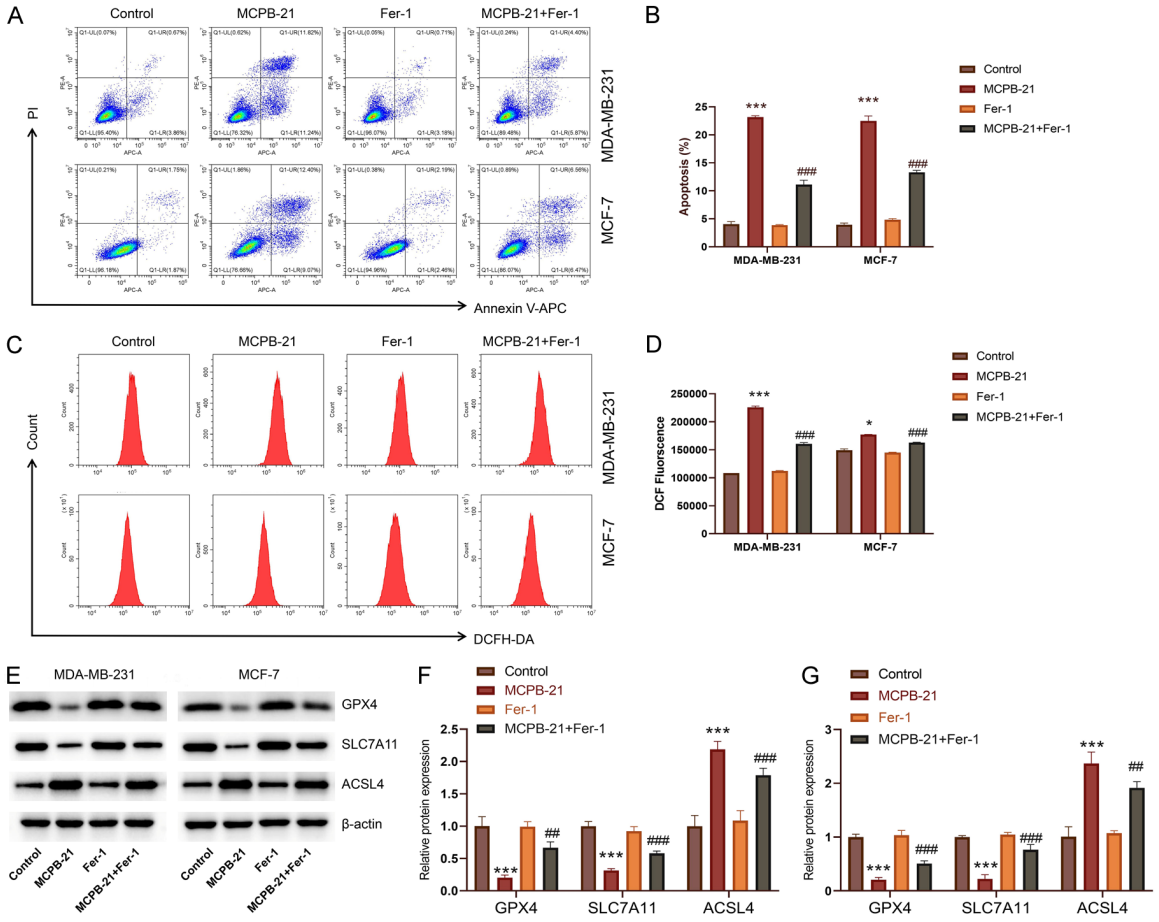

Figure 7. MCPB-21 induces cell death in breast cancer cell lines MDA-MB-231 and MCF-7 *via* the ferroptosis pathway. (A, B) Flow cytometry analysis of cell death rates in each group, along with statistical analysis. (C, D) Detection of intracellular ROS levels in each group using the DCFH-DA fluorescent probe *via* flow cytometry, along with statistical analysis. (E) Representative Western blots for GPX4, SLC7A11, and ACSL4. Quantitative analysis of the expression levels of the aforementioned proteins in MDA-MB-231 (F) and MCF-7 (G) cells. Compared with the Control group: $*P < 0.05$, $**P < 0.001$. Compared with the MCPB-21 group: $\#\#P < 0.01$, $\#\#\#P < 0.001$.

Fer-1, ROS production was effectively inhibited. This result confirms that MCPB-21 is capable of inducing ferroptosis by triggering an oxidative stress response. Furthermore, compared to the control group, MCPB-21 downregulated the protein expression levels of GPX4 and SLC7A11 while upregulating ACSL4. When combined with Fer-1, these alterations in protein expression were reversed to varying degrees (**Figure 7E-G**). In summary, MCPB-21 induces ferroptosis in breast cancer cells by downregulating GPX4 and SLC7A11 and upregulating ACSL4, thereby leading to the abnormal accumulation of ROS.

Analysis of the anti-breast cancer activity of MCPB-21 in transplanted tumor experiments

The results of nude mouse tumor formation experiments showed that compared with the control group, 10 and 40 mg/kg MCPB-21 could inhibit tumor growth, which was better than 10 mg/kg CBD (**Figure 8A** and **8B**). The values of xenografted tumor showed that the volume of xenografted tumor decreased after MCPB-21 and CBD treatment (**Figure 8C**). The maximum volume of the xenograft tumors was 692 mm^3, with a diameter of 9.99 mm. H&E staining results showed that compared with the control group, focal necrosis occurred in the tumor tissues of the MCPB-21 and CBD treatment groups. The tumor cells in the necrotic foci disintegrated, the nuclei condensed and fragmented, and the cytoplasm dissolved (**Figure 8D**). Immunohistochemistry results showed that compared with the control group, MCPB-21, and CBD could inhibit the level of Ki67, and the expression of Ki67 was the lowest in the 40 mg/kg MCPB-21 treatment group.

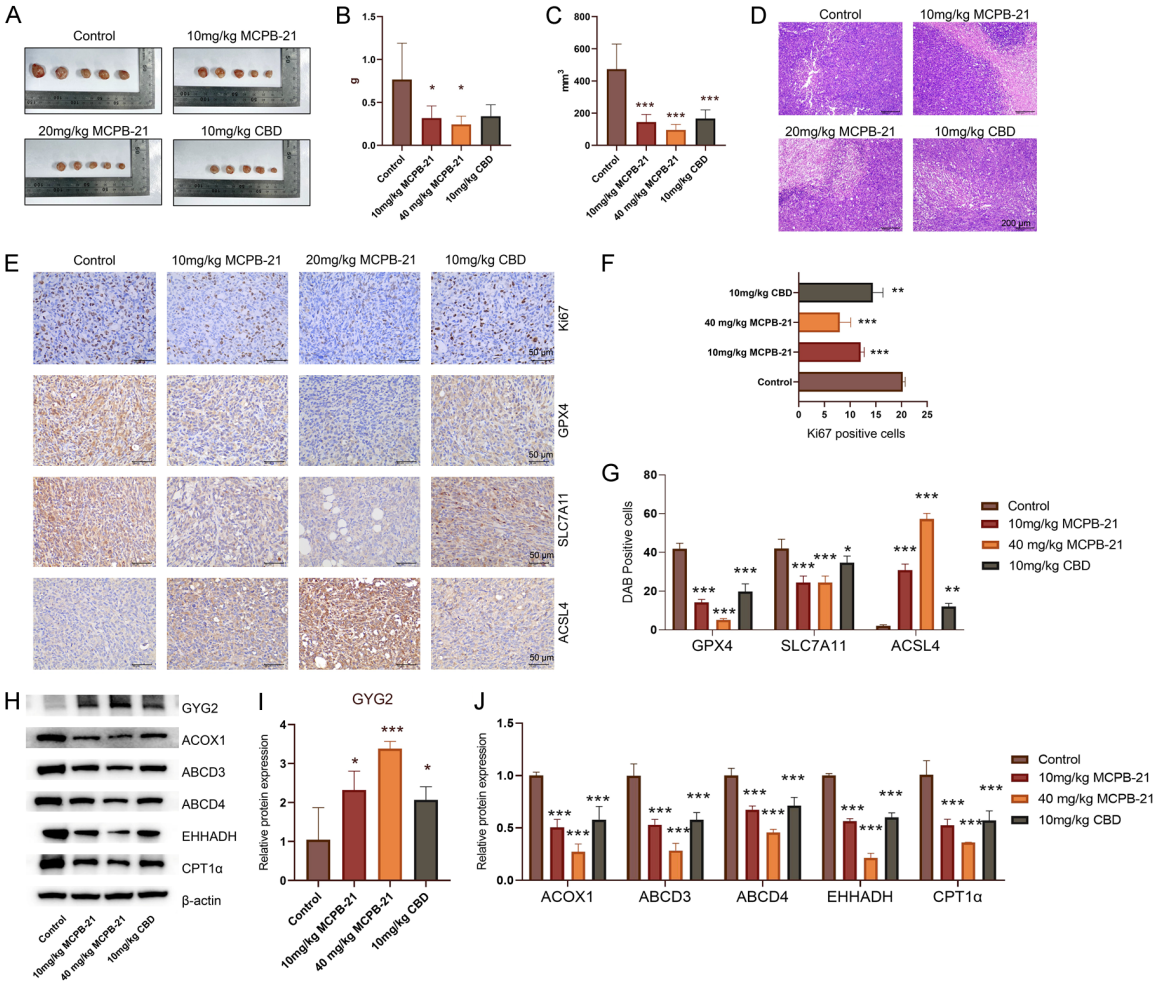

Figure 8. Effects of CBD and MCPB-21 on the formation of transplant tumors in MDA-AB-231. A. Mouse transplantation tumor. B. Weight of transplant tumor. C. The values of xenografted tumor volumes. D. H&E staining. E. Representative immunohistochemistry images of Ki67, GPX4, SLC7A11, and ACSL4. F. Statistical results of Ki67. G. Statistical results of GPX4, SLC7A11, and ACSL4 expression. H. Representative bands of GYG2, ACOX1, ABCD3, ABCD4, EHHADH, and CPT1a. I. Relative expression of GYG2. J. Relative expression of ACOX1, ABCD3, ABCD4, EHHADH, and CPT1a. Compared with the control group, $*P < 0.05$, $**P < 0.01$, and $***P < 0.001$.

As for GPX4, SLC7A11, and ACSL4, compared with the control group, MCPB-21, and CBD inhibited the expression of GPX4 and SLC7A11 and upregulated ACSL4 (**Figure 8E-G**). Notably, MCPB-21 and CBD upregulated the expression of GYG2, while inhibiting the expression of ACOX1, ABCD3, ABCD4, EHHADH, and CPT1α in MDA-AB-231 transplanted tumors (**Figure 8H-J**). This ensemble of data underlines that the CBD derivative MCPB-21 has a stronger anti-tumor capacity, predominantly *via* the modulation of the fatty acid β-oxidation-mediated ferroptosis.

Discussion

Breast cancer remains one of the predominant causes of cancer-related mortality globally, with its incidence rising annually, particularly among young and middle-aged women [37, 38]. Its incidence is expected to increase by more than 46% by 2040 and will constitute nearly one-third of all new cancer diagnoses in women [38]. Current therapeutic modalities primarily encompass surgery, chemotherapy, endocrine therapy, and targeted drug treatments. Furthermore, identifying key molecular markers involved in the initiation and progression of tumors has become a crucial means for precisely assessing the efficacy of immunotherapy and exploring the mechanisms of cell death [39, 40]. However, the emergence of drug resistance poses a significant challenge, undermining treatment effectiveness and diminishing patient survival rates [6]. Consequently, there

is a pressing need to identify and develop novel therapeutic targets and pharmacological agents to circumvent drug resistance, thereby enhancing treatment outcomes and improving the prognosis and quality of life for breast cancer patients. This underscores the critical importance of advancing drug development in the management of breast cancer.

Active molecules derived from natural Chinese medicinal herbs are widely utilized in basic medical research [41]. CBD is a pure natural ingredient extracted from the cannabis plant and is one of the most widely studied phytocannabinoids [42]. As research deepens, in addition to its anti-inflammatory, antiemetic, and analgesic effects, CBD's anti-tumor activity has attracted increasing attention [43, 44]. Cell proliferation is regulated by the cell cycle, and blocking the division cycle of tumor cells is an important anti-tumor mechanism. Studies have confirmed that CBD has a cell cycle-regulating effect on many types of cancer, such as thyroid cancer and breast cancer cells, pancreatic cancer, gastric cancer [25, 45-47]. Although CBD has certain anti-tumor effects by inducing cell cycle arrest and autophagy, promoting cell apoptosis, regulating angiogenesis, and inhibiting tumor cell migration and invasion, its simple structure, poor water solubility, low bioavailability, and significant inhibition of its antioxidant properties and stability limit its clinical application, so structural optimization is urgently needed. Our research team has previously modified CBD, established a library of cannabidiol derivatives, and screened out a new compound MCPB-21, which has been proven to have the effect of treating breast cancer. The synthesis of MCPB-21 follows the principles of the Mannich reaction. This strategy constitutes a well-established method for the structural diversification of natural phenolic compounds, aimed at enhancing their biological activity and water solubility [48]. In breast cancer cells MDA-AB-231 and MCF-7, MCPB-21 was able to induce apoptosis and inhibit the invasiveness of tumor cells at concentrations of 5, 10, and 20 μM. In addition, the formation of lipid droplets was observed after treatment, suggesting that fatty acid metabolism was inhibited and metabolic reprogramming of cells occurred. Flow cytometry results showed that MCPB-21 treatment enhanced the production of ROS, which may exert anti-tumor effects by inducing oxidative stress. Therefore, MCPB-21 has multiple effects of promoting tumor cell apoptosis, enhancing ROS levels, and regulating fat metabolism, showing potential anti-tumor effects.

Bioinformatics analysis revealed a significant downregulation of GYG2 in the cancerous tissues of breast cancer patients, with a notable reduction in survival rates among those exhibiting low GYG2 expression. This suggests a potential anti-cancer role for GYG2 in the pathogenesis of breast cancer. Furthermore, building on previous findings that MCPB-21 inhibits the proliferation of breast cancer cells, we employed molecular docking techniques to examine the interaction between MCPB-21 and GYG2. The analysis demonstrated that MCPB-21 forms a stable complex with GYG2, characterized by a binding energy of -10 kcal/mol, indicating that MCPB-21 may exert its anti-tumor effects through its interaction with GYG2. GYG2 is an auto-glucosylation protein involved in glycogen biosynthesis, which facilitates the metabolism of glucose and galactose [49]. Notably, tumor cells exhibit elevated expression of glucose transporters, such as GLUT1, enabling them to uptake substantial quantities of glucose to supply energy and biosynthetic precursors necessary for rapid proliferation [50]. Moreover, fatty acid metabolism is intricately linked to tumorigenesis. Recent studies indicate that the energy derived from fatty acids in cancer cells may enhance tumor initiation, progression, and metastasis [51, 52]. Furthermore, the knockdown of GYG2 in adipocytes resulted in a concurrent decrease in the expression of the peroxidase ACOX1, suggesting that GYG2 may play a regulatory role in the expression of ACOX1, a rate-limiting enzyme in peroxisomal fatty acid β-oxidation [12]. Conversely, research on glycogen dynamics in adipocyte differentiation revealed that inhibiting glycogen production significantly reduces lipid droplet formation [11], implying that suppression of GYG2 expression may hinder the formation of intracellular lipid droplets. Lipid droplets serve as storage organelles for fatty acids, and the promotion of fatty acid β-oxidation is known to decrease the intracellular lipid droplet content [53].

Fatty acid metabolism is a crucial link in lipid metabolism, not only being essential for the

growth and development of normal cells, but also playing a significant role in tumor occurrence, progression, and metastasis [54]. Compared to normal cells, tumor cells exhibit accelerated proliferation and increased energy demands, and their energy production is closely related to the metabolic process [55]. Fatty acid metabolism is particularly closely related to tumor development. Recent studies have shown that the energy derived from fatty acids in cancer cells may promote tumor occurrence, progression, and metastasis [56]. ACOX1 catalyzes the initial oxidation of long-chain fatty acids; ABCD3 and ABCD4 are responsible for fatty acid transport; EHHADH is located in the mitochondrial matrix and plays a key role in the β-oxidation pathway; and CPT1α is located on the outer mitochondrial membrane and regulates the entry of fatty acids into mitochondria for subsequent oxidation [57, 58]. These enzymes jointly regulate the β-oxidation pathway of fatty acids. This study found that after treatment with MCPB-21, the expression of ACOX1, ABCD3, ABCD4, EHHADH, and CPT1α in breast cancer cells was significantly reduced. Additionally, the combination of MCPB-21 and 12-tricosadiynoic acid (12-Tricosadiynoic acid) with GYG2 gene silencing further led to a decrease in the protein expression levels of these enzymes. This indicates that the β-oxidation function of fatty acids is inhibited, which in turn causes intracellular lipid accumulation and oxidative stress, ultimately inducing ferroptosis and demonstrating potential antitumor effects.

Recent studies [59] have shown that breast cancer cells exhibit significant metabolic plasticity. Unlike normal cells, cancer cells rely on FAO to generate energy and maintain redox homeostasis [60]. Our research has found that MCPB-21 inhibits FAO by targeting GYG2; this effect not only blocks the energy supply of the tumor but also disrupts lipid homeostasis, thereby creating necessary conditions for inducing ferroptosis.

Lipid metabolism reprogramming has been proven to be not only a metabolic marker of malignant tumors but also a core molecular switch that regulates ferroptosis, a new type of cell death [61]. Ferroptosis is characterized by the accumulation of iron and ROS [62]. The ferroptosis process mainly includes the destruction of iron metabolism leading to the induction of the Fenton reaction, imbalance of redox homeostasis, and the triggering of lipid peroxidation, which ultimately leads to cell membrane damage and cell death [63]. GPX4 is the main antioxidant enzyme that can reduce lipid peroxides and inhibit ferroptosis [64]. SLC7A11 is responsible for thiothreitol uptake, synthesis of glutathione (GSH), and protection of cells from oxidative stress-induced lipid peroxidation [65]. ACSL4 regulates lipid metabolism, promotes lipid peroxidation, and is a triggering factor of ferroptosis [66]. Moreover, GPX4 and SLC7A11 are often upregulated in breast cancer, which helps cell anti-oxidation and survival and may be related to treatment resistance [67, 68]. ACSL4 is frequently regarded as a biomarker for ferroptosis, with its upregulation potentially facilitating lipid peroxidation and subsequent cell death [69]. *In vitro* studies have demonstrated that MCPB-21 can inhibit GPX4 and SLC7A11, while simultaneously upregulating ACSL4 *via* GYG2. The *in vivo* experiments further demonstrated that MCPB-21 and CBD could enhance lipid peroxidation by down-regulating antioxidant proteins GPX4 and SLC7A11 and up-regulating the enzyme ACSL4, thereby inducing ferroptosis and exerting anti-tumor effects. As a derivative of CBD, MCPB-21 exhibited stronger anti-tumor efficacy, which was related to its regulatory role in the ferroptosis process mediated by fatty acid β-oxidation.

Conclusion

In summary, this study confirmed that MCPB-21 can inhibit breast cancer cell invasion and promote apoptosis through *in vitro* and *in vivo* experiments. Mechanism analysis found that MCPB-21 inhibits fatty acid β-oxidation by targeting GYG2 to inhibit ACOX1, leading to ROS enrichment and inducing ferroptosis of breast cancer cells. This study provides a new direction and theoretical basis for anticancer drugs. However, utilizing biological or biophysical methods to validate the direct binding affinity between MCPB-21 and GYG2 and constructing a robust gene rescue model will be the primary focus of future research.

Disclosure of conflict of interest

None.

Address correspondence to: Dr. Jing Li, Department of General Internal Medicine, Sichuan Cancer Hospital and Institute, Sichuan Cancer Center, School of Medicine, University of Electronic Science and Technology of China, 55 Renmin South Road, Wuhou District, Chengdu 610041, Sichuan, China. E-mail: lijing@scszlyy.org.cn; Dr. Bin Liu, Department of Medical Oncology, Sichuan Cancer Hospital and Institute, Sichuan Cancer Center, Affiliated Cancer Hospital of University of Electronic Science and Technology of China, 55 Renmin South Road, Wuhou District, Chengdu 610041, Sichuan, China. E-mail: liubin@scszlyy.org.cn

References

[1] Sung H, Wiese D, Jatoi I and Jemal A. State variation in racial and ethnic disparities in incidence of triple-negative breast cancer among US women. JAMA Oncol 2023; 9: 700-704.

[2] Li RQ, Zhao XH, Zhu Q, Liu T, Hondermarck H, Thorne RF, Zhang XD and Gao JN. Exploring neurotransmitters and their receptors for breast cancer prevention and treatment. Theranostics 2023; 13: 1109-1129.

[3] Miao H, Verkooijen HM, Chia KS, Bouchardy C, Pukkala E, Larønningen S, Mellemkjær L, Czene K and Hartman M. Incidence and outcome of male breast cancer: an international population-based study. J Clin Oncol 2011; 29: 4381-4386.

[4] Konduri S, Singh M, Bobustuc G, Rovin R and Kassam A. Epidemiology of male breast cancer. Breast 2020; 54: 8-14.

[5] Dobato Portoles O, Aparicio Lopez D, Ibañez Carreras R, Aguirre Ortega E, Eizaguirre Zarza B, García Mur C, Carrasquer Puyal A, Cebollero Benito MP, Comín Novella LI, Allue Cabañuz M, Martinez Ubieto F, Sousa Domínguez R, Torcal Aznar J and Casamayor Franco C. Male breast cancer: a multicenter study in Aragon over 27 years. Cir Esp (Engl Ed) 2024; 102: 524-532.

[6] Kumar H, Gupta NV, Jain R, Madhunapantula SV, Babu CS, Kesharwani SS, Dey S and Jain V. A review of biological targets and therapeutic approaches in the management of triple-negative breast cancer. J Adv Res 2023; 54: 271-292.

[7] Li Y, Zhang H, Merkher Y, Chen L, Liu N, Leonov S and Chen Y. Recent advances in therapeutic strategies for triple-negative breast cancer. J Hematol Oncol 2022; 15: 121.

[8] Zhai L, Mu J, Zong H, DePaoli-Roach AA and Roach PJ. Structure and chromosomal localization of the human glycogenin-2 gene GYG2. Gene 2000; 242: 229-235.

[9] Vardanyan S, Brosig A, Merz H, Ranjbar M, Kakkassery V, Grisanti S and Tura A. Metastasis of uveal melanoma with monosomy-3 is associated with a less glycogenetic gene expression profile and the dysregulation of glycogen storage. Cancers (Basel) 2020; 12: 2101.

[10] Li N, Torres MB, Spetz MR, Wang R, Peng L, Tian M, Dower CM, Nguyen R, Sun M, Tai CH, de Val N, Cachau R, Wu X, Hewitt SM, Kaplan RN, Khan J, St Croix B, Thiele CJ and Ho M. CAR T cells targeting tumor-associated exons of glypican 2 regress neuroblastoma in mice. Cell Rep Med 2021; 2: 100297.

[11] Mayeuf-Louchart A, Lancel S, Sebti Y, Pourcet B, Loyens A, Delhaye S, Duhem C, Beauchamp J, Ferri L, Thorel Q, Boulinguiez A, Zecchin M, Dubois-Chevalier J, Eeckhoute J, Vaughn LT, Roach PJ, Dani C, Pederson BA, Vincent SD, Staels B and Duez H. Glycogen dynamics drives lipid droplet biogenesis during brown adipocyte differentiation. Cell Rep 2019; 29: 1410-1418, e1416.

[12] Ham M, Cho Y, Kang TW, Oh T, Kim HJ and Kim KH. Transcriptome-wide analysis reveals GYG_2 as a mitochondria-related aging biomarker in human subcutaneous adipose tissue. Aging Cell 2024; 23: e14049.

[13] Yao X, Xie R, Cao Y, Tang J, Men Y, Peng H and Yang W. Simvastatin induced ferroptosis for triple-negative breast cancer therapy. J Nanobiotechnology 2021; 19: 311.

[14] Vander Heiden MG, Cantley LC and Thompson CB. Understanding the Warburg effect: the metabolic requirements of cell proliferation. Science 2009; 324: 1029-1033.

[15] Zaidi N, Lupien L, Kuemmerle NB, Kinlaw WB, Swinnen JV and Smans K. Lipogenesis and lipolysis: the pathways exploited by the cancer cells to acquire fatty acids. Prog Lipid Res 2013; 52: 585-589.

[16] Jin HR, Wang J, Wang ZJ, Xi MJ, Xia BH, Deng K and Yang JL. Lipid metabolic reprogramming in tumor microenvironment: from mechanisms to therapeutics. J Hematol Oncol 2023; 16: 103.

[17] Duncan OF, Granat L, Ranganathan R, Singh VK, Mazaud D, Fanto M, Chambers D, Ballard CG and Bateman JM. Ras-ERK-ETS inhibition alleviates neuronal mitochondrial dysfunction by reprogramming mitochondrial retrograde signaling. PLoS Genet 2018; 14: e1007567.

[18] Jiang X, Peng Q, Peng M, Oyang L, Wang H, Liu Q, Xu X, Wu N, Tan S, Yang W, Han Y, Lin J, Xia L, Tang Y, Luo X, Dai J, Zhou Y and Liao Q. Cellular metabolism: a key player in cancer ferroptosis. Cancer Commun (Lond) 2024; 44: 185-204.

[19] Lei G, Zhang Y, Koppula P, Liu X, Zhang J, Lin SH, Ajani JA, Xiao Q, Liao Z, Wang H and Gan B. The role of ferroptosis in ionizing radiation-induced cell death and tumor suppression. Cell Res 2020; 30: 146-162.

[20] Zou Y, Zheng S, Xie X, Ye F, Hu X, Tian Z, Yan SM, Yang L, Kong Y, Tang Y, Tian W, Xie J, Deng X, Zeng Y, Chen ZS, Tang H and Xie X. N6-methyladenosine regulated FGFR4 attenuates ferroptotic cell death in recalcitrant HER2-positive breast cancer. Nat Commun 2022; 13: 2672.
[21] Newman DJ. Natural products and drug discovery. Natl Sci Rev 2022; 9: nwac206.
[22] Zhang L, Song J, Kong L, Yuan T, Li W, Zhang W, Hou B, Lu Y and Du G. The strategies and techniques of drug discovery from natural products. Pharmacol Ther 2020; 216: 107686.
[23] McAllister SD, Murase R, Christian RT, Lau D, Zielinski AJ, Allison J, Almanza C, Pakdel A, Lee J, Limbad C, Liu Y, Debs RJ, Moore DH and Desprez PY. Pathways mediating the effects of cannabidiol on the reduction of breast cancer cell proliferation, invasion, and metastasis. Breast Cancer Res Treat 2011; 129: 37-47.
[24] Laezza C, Pagano C, Navarra G, Pastorino O, Proto MC, Fiore D, Piscopo C, Gazzerro P and Bifulco M. The endocannabinoid system: a target for cancer treatment. Int J Mol Sci 2020; 21: 747.
[25] Sreevalsan S, Joseph S, Jutooru I, Chadalapaka G and Safe SH. Induction of apoptosis by cannabinoids in prostate and colon cancer cells is phosphatase dependent. Anticancer Res 2011; 31: 3799-3807.
[26] Franco V, Gershkovich P, Perucca E and Bialer M. The interplay between liver first-pass effect and lymphatic absorption of cannabidiol and its implications for cannabidiol oral formulations. Clin Pharmacokinet 2020; 59: 1493-1500.
[27] Rooney TA, Carpenter JW, KuKanich B, Gardhouse SM, Magnin GC and Tully TN. Feeding decreases the oral bioavailability of cannabidiol and cannabidiolic acid in hemp oil in New Zealand White rabbits (oryctolagus cuniculus). Am J Vet Res 2022; 83: ajvr.22.01.0006.
[28] Martin BJ and van Golen KL. A comparison of cholesterol uptake and storage in inflammatory and noninflammatory breast cancer cells. Int J Breast Cancer 2012; 2012: 412581.
[29] Lai Q, Yang CJ, Zhang Q, Zhuang M, Ma YH, Lin CY, Zeng GZ and Yin JL. Alkaloid from *Alstonia yunnanensis* diels root against gastrointestinal cancer: acetoxytabernosine inhibits apoptosis in hepatocellular carcinoma cells. Front Pharmacol 2023; 13: 1085309.
[30] Elbaz M, Nasser MW, Ravi J, Wani NA, Ahirwar DK, Zhao H, Oghumu S, Satoskar AR, Shilo K, Carson WE 3rd and Ganju RK. Modulation of the tumor microenvironment and inhibition of EGF/EGFR pathway: novel anti-tumor mechanisms of Cannabidiol in breast cancer. Mol Oncol 2015; 9: 906-919.
[31] Weber EM, Zidar J, Ewaldsson B, Askevik K, Udén E, Svensk E and Törnqvist E. Aggression in group-housed male mice: a systematic review. Animals (Basel) 2022; 13: 143.
[32] Lidster K, Owen K, Browne WJ and Prescott MJ. Cage aggression in group-housed laboratory male mice: an international data crowdsourcing project. Sci Rep 2019; 9: 15211.
[33] Shi ZY, Ding ZR, Huang YL, Lei YR, Huang HB, Qing Y, Deng MR, Lu XM, Dong XD, Xia LJ, Xu S, Zhong XG, Li L, Kong FB and Wang XT. Silencing of SIVA-1 promotes cisplatin resistance in gastric cancer via the Bcl-2/BAX-mediated mitochondria-dependent apoptosis pathway. Oncol Rep 2026; 55: 95.
[34] Workman P, Aboagye EO, Balkwill F, Balmain A, Bruder G, Chaplin DJ, Double JA, Everitt J, Farningham DA, Glennie MJ, Kelland LR, Robinson V, Stratford IJ, Tozer GM, Watson S, Wedge SR and Eccles SA; Committee of the National Cancer Research Institute. Guidelines for the welfare and use of animals in cancer research. Br J Cancer 2010; 102: 1555-1577.
[35] Wang J, Li T, Yue C, Zhong S, Yang X, Li J and Li Y. Preparation of nanoparticles of β-cyclodextrin-loaded scutellarein anti-tumor activity research by targeting integrin αvβ3. Cancer Nanotechnol 2021; 12: 29.
[36] Yuan-Ce L, Qi Z, Hong-Yang Z, Yan-Wen W, Yu-Mei S, Bi-Juan Y and Jun-Lin Y. Artesunate, as an Hsp90 inhibitor, inhibits the proliferation of Burkitt's lymphoma cells by inhibiting AKT and ERK. Front Pharmacol 2023; 14: 1218467.
[37] Price S, Long AF and Godfrey M. What is traditional acupuncture--exploring goals and processes of treatment in the context of women with early breast cancer. BMC Complement Altern Med 2014; 14: 201.
[38] Nguyen YT, To NB, Truong VN, Kim HY, Ediriweera MK, Lim Y and Cho SK. Impairment of glucose metabolism and suppression of stemness in MCF-7/SC human breast cancer stem cells by nootkatone. Pharmaceutics 2022; 14: 906.
[39] Yu Y, Chen H, Ouyang W, Zeng J, Huang H, Mao L, Jia X, Guan T, Wang Z, Lin R, Huang Z, Yin H, Yao H and Zhang K. Unraveling the role of M1 macrophage and CXCL9 in predicting immune checkpoint inhibitor efficacy through multicohort analysis and single-cell RNA sequencing. MedComm (2020) 2024; 5: e471.
[40] Ouyang W, Lai Z, Huang H and Ling L. Machine learning-based identification of cuproptosis-related lncRNA biomarkers in diffuse large B-cell lymphoma. Cell Biol Toxicol 2025; 41: 72.
[41] Ouyang W, Deng Z, Li Y, Chi W, Huang Z, Zhan C, Li M, Wang D, Li F, Liu Y and Ling L. Traditional Chinese medicine in cerebral in-

farction: integrative strategies and future directions. Phytomedicine 2025; 143: 156841.
[42] Rosenberg EC, Chamberland S, Bazelot M, Nebet ER, Wang X, McKenzie S, Jain S, Greenhill S, Wilson M, Marley N, Salah A, Bailey S, Patra PH, Rose R, Chenouard N, Sun SED, Jones D, Buzsáki G, Devinsky O, Woodhall G, Scharfman HE, Whalley BJ and Tsien RW. Cannabidiol modulates excitatory-inhibitory ratio to counter hippocampal hyperactivity. Neuron 2023; 111: 1282-1300, e1288.
[43] Peyravian N, Deo S, Daunert S and Jimenez JJ. The anti-inflammatory effects of cannabidiol (CBD) on acne. J Inflamm Res 2022; 15: 2795-2801.
[44] Russo C, Lavorgna M, Nugnes R, Orlo E and Isidori M. Comparative assessment of antimicrobial, antiradical and cytotoxic activities of cannabidiol and its propyl analogue cannabidivarin. Sci Rep 2021; 11: 22494.
[45] Misri S, Kaul K, Mishra S, Charan M, Verma AK, Barr MP, Ahirwar DK and Ganju RK. Cannabidiol inhibits tumorigenesis in cisplatin-resistant non-small cell lung cancer *via* TRPV2. Cancers (Basel) 2022; 14: 1181.
[46] Hamad H and Olsen BB. Cannabidiol induces cell death in human lung cancer cells and cancer stem cells. Pharmaceuticals (Basel) 2021; 14: 1169.
[47] Kisková T, Mungenast F, Suváková M, Jäger W and Thalhammer T. Future aspects for cannabinoids in breast cancer therapy. Int J Mol Sci 2019; 20: 1673.
[48] Meng Y, Wang Y, Li S, Cai Z, Zhuang G and Yang Y. Design, synthesis, and antitumor activity of novel eupatilin derivatives based on the Mannich reaction. Chem Pharm Bull (Tokyo) 2025; 73: 112-120.
[49] Mu J and Roach PJ. Characterization of human glycogenin-2, a self-glucosylating initiator of liver glycogen metabolism. J Biol Chem 1998; 273: 34850-34856.
[50] Reckzeh ES, Karageorgis G, Schwalfenberg M, Ceballos J, Nowacki J, Stroet MCM, Binici A, Knauer L, Brand S, Choidas A, Strohmann C, Ziegler S and Waldmann H. Inhibition of glucose transporters and glutaminase synergistically impairs tumor cell growth. Cell Chemical Biology 2019; 26: 1214-1228, e1225.
[51] Hoy AJ, Nagarajan SR and Butler LM. Tumour fatty acid metabolism in the context of therapy resistance and obesity. Nat Rev Cancer 2021; 21: 753-766.
[52] Xiang W, Lv H, Xing F, Sun X, Ma Y, Wu L, Lv G, Zong Q, Wang L, Wu Z, Feng Q, Yang W and Wang H. Inhibition of ACLY overcomes cancer immunotherapy resistance *via* polyunsaturated fatty acids peroxidation and cGAS-STING activation. Sci Adv 2023; 9: eadi2465.
[53] Ariyoshi K, Nishiyama K, Kato Y, Mi X, Ito T, Azuma YT, Nishimura A and Nishida M. Inhibition of Drp1-filamin protein complex prevents hepatic lipid droplet accumulation by increasing mitochondria-lipid droplet contact. Int J Mol Sci 2024; 25: 5446.
[54] Luo X, Cheng C, Tan Z, Li N, Tang M, Yang L and Cao Y. Emerging roles of lipid metabolism in cancer metastasis. Molecular Cancer 2017; 16: 76.
[55] Wang H, Xi Q and Wu G. Fatty acid synthase regulates invasion and metastasis of colorectal cancer *via* Wnt signaling pathway. Cancer Med 2016; 5: 1599-1606.
[56] Currie E, Schulze A, Zechner R, Walther TC and Farese RV Jr. Cellular fatty acid metabolism and cancer. Cell Metab 2013; 18: 153-161.
[57] Tang S, Wu F, Lin X, Gui W, Zheng F and Li H. The effects of new selective PPARα agonist CP775146 on systematic lipid metabolism in obese mice and its potential mechanism. J Diabetes Res 2020; 2020: 4179852.
[58] Chung KW, Lee EK, Lee MK, Oh GT, Yu BP and Chung HY. Impairment of PPARα and the fatty acid oxidation pathway aggravates renal fibrosis during aging. J Am Soc Nephrol 2018; 29: 1223-1237.
[59] Simões RV, Serganova IS, Kruchevsky N, Leftin A, Shestov AA, Thaler HT, Sukenick G, Locasale JW, Blasberg RG, Koutcher JA and Ackerstaff E. Metabolic plasticity of metastatic breast cancer cells: adaptation to changes in the microenvironment. Neoplasia 2015; 17: 671-684.
[60] Meng Y, Guo D, Lin L, Zhao H, Xu W, Luo S, Jiang X, Li S, He X, Zhu R, Shi R, Xiao L, Wu Q, He H, Tao J, Jiang H, Wang Z, Yao P, Xu D and Lu Z. Glycolytic enzyme PFKL governs lipolysis by promoting lipid droplet-mitochondria tethering to enhance β-oxidation and tumor cell proliferation. Nat Metab 2024; 6: 1092-1107.
[61] Koundouros N and Poulogiannis G. Reprogramming of fatty acid metabolism in cancer. Br J Cancer 2020; 122: 4-22.
[62] Zheng D, Liu J, Piao H, Zhu Z, Wei R and Liu K. ROS-triggered endothelial cell death mechanisms: focus on pyroptosis, parthanatos, and ferroptosis. Front Immunol 2022; 13: 1039241.
[63] Zheng J and Conrad M. The metabolic underpinnings of ferroptosis. Cell Metab 2020; 32: 920-937.
[64] Forcina GC and Dixon SJ. GPX4 at the crossroads of lipid homeostasis and ferroptosis. Proteomics 2019; 19: e1800311.
[65] Pan CF, Wei K, Ma ZJ, He YZ, Huang JJ, Guo ZZ, Chen ZP, Barr MP, Shackelford RE, Xia Y and Wang J. CircP4HB regulates ferroptosis *via* SLC7A11-mediated glutathione synthesis in

lung adenocarcinoma. Transl Lung Cancer Res 2022; 11: 366-380.
[66] He F, Huang X, Wei G, Lin X, Zhang W, Zhuang W, He W, Zhan T, Hu H and Yang H. Regulation of ACSL4-catalyzed lipid peroxidation process resists cisplatin ototoxicity. Oxid Med Cell Longev 2022; 2022: 3080263.
[67] Ouyang S, Li H, Lou L, Huang Q, Zhang Z, Mo J, Li M, Lu J, Zhu K, Chu Y, Ding W, Zhu J, Lin Z, Zhong L, Wang J, Yue P, Turkson J, Liu P, Wang Y and Zhang X. Inhibition of STAT3-ferroptosis negative regulatory axis suppresses tumor growth and alle*via*tes chemoresistance in gastric cancer. Redox Biol 2022; 52: 102317.
[68] Stockwell BR. Ferroptosis turns 10: emerging mechanisms, physiological functions, and therapeutic applications. Cell 2022; 185: 2401-2421.
[69] Yuan H, Li X, Zhang X, Kang R and Tang D. Identification of ACSL4 as a biomarker and contributor of ferroptosis. Biochem Biophys Res Commun 2016; 478: 1338-1343.